






The impact of environment on the lives of disc galaxies as revealed by SDSS-IV MaNGA

Shuang Zhou ¹★, Michael Merrifield ¹, Alfonso Aragón-Salamanca ¹, Joel R. Brownstein ²,
Niv Drory,³ Renbin Yan ⁴ and Richard R. Lane⁵

¹*School of Physics & Astronomy, University of Nottingham, University Park, Nottingham NG7 2RD, UK*

²*Department of Physics and Astronomy, University of Utah, 115 S. 1400 E., Salt Lake City, UT 84112, USA*

³*McDonald Observatory, The University of Texas at Austin, 1 University Station, Austin, TX 78712, USA*

⁴*Department of Physics, The Chinese University of Hong Kong, Shatin, N.T., Hong Kong, SAR 999077, China*

⁵*Centro de Investigación en Astronomía, Universidad Bernardo O'Higgins, Avenida Viel 1497, Santiago, Chile*

Accepted 2022 October 5. Received 2022 October 4; in original form 2022 August 8

ABSTRACT

Environment has long been known to have significant impact on the evolution of galaxies, but here we seek to quantify the subtler differences that might be found in disc galaxies, depending on whether they are isolated, the most massive galaxy in a group (centrals), or a lesser member (satellites). The MaNGA survey allows us to define a large mass-matched sample of 574 galaxies with high-quality integrated spectra in each category. Initial examination of their spectral indices indicates significant differences, particularly in low-mass galaxies. Semi-analytic spectral fitting of a full chemical evolution model to these spectra confirms these differences, with low-mass satellites having a shorter period of star formation and chemical enrichment typical of a closed box, while central galaxies have more extended histories, with evidence of ongoing gas accretion over their lifetimes. The derived parameters for gas infall time-scale and wind strength suggest that low-mass satellite galaxies have their hot haloes of gas effectively removed, while central galaxies retain a larger fraction of gas than isolated galaxies due to the deeper group potential well in which they sit. S0 galaxies form a distinct subset within the sample, particularly at higher masses, but do not bias the inferred lower mass environmental impact significantly. The consistent picture that emerges underlines the wealth of archaeological information that can be extracted from high-quality spectral data using techniques like semi-analytic spectral fitting.

Key words: galaxies: evolution – galaxies: formation – galaxies: fundamental parameters – galaxies: stellar content.

1 INTRODUCTION

Galaxies are complex systems, and their formation and evolution are affected by a variety of processes. In the current paradigm, galaxies form at the centre of dark matter haloes whose formation and evolution are described by the Lambda cold dark matter cosmology (White & Rees 1978). Baryonic matter accretes into these dark matter haloes, fuelling star formation. During this initial gas accretion and subsequent evolution, galaxies can experience a wide range of interactions with their environment, on scales ranging from mergers with individual galaxies to hydrodynamic interactions with galaxy clusters and the cosmic web.

It is therefore perhaps unsurprising that galaxy properties depend on the environment that they inhabit. Most famously, high-density regions such as groups and clusters contain a significantly higher fraction of red galaxies, often associated with earlier morphological types (e.g. Oemler 1974; Dressler 1980; Postman & Geller 1984). With the advent of large-scale surveys such as the Sloan Digital Sky Survey (SDSS; York et al. 2000), the environmental dependence of the galaxies' star formation histories (SFHs) has

been extensively explored. Such surveys have revealed that satellite galaxies in groups and clusters (e.g. Pasquali et al. 2010; Peng et al. 2012; Wetzel, Tinker & Conroy 2012; Wetzel et al. 2013) and galaxies that live in high-density regions (e.g. Kauffmann et al. 2003; Baldry et al. 2006) are more likely to have their star formation quenched than isolated galaxies. Other properties related to the galaxies' SFHs show related environmental dependence: galaxies are redder (Blanton et al. 2005b; Li et al. 2006) and have a higher 4000 Å break strength (Kauffmann et al. 2004; Li et al. 2006) in denser environments. Further observations have shown that this environmental dependence may persist to high redshifts (e.g. Peng et al. 2010; Darvish et al. 2016; Kawinwanichakij et al. 2017). More recently, spatially resolved observations allow the investigation of such environmental effects within the galaxies themselves, although several studies indicate that the environment seems to work mainly globally, with very little effect on the radial profiles of stellar population properties (e.g. Zheng et al. 2017; Spindler et al. 2018).

There is some evidence that, in addition to affecting the star formation activity of galaxies, the environment may also impact on their chemical evolution, although the effects seem more subtle, complex, and uncertain. Early-type galaxies in low-density environments are more metal rich than their counterparts in high-density environments

* E-mail: shuang.zhou@nottingham.ac.uk

(Sánchez-Blázquez et al. 2006). Further, Pasquali et al. (2010) found that satellite galaxies seem to be more enriched in metals than central ones, especially in low-mass systems. However, the opposite trend was found by Zheng et al. (2017): In large-scale sheets and voids, satellite galaxies are relatively more metal poor than central ones. Zheng et al. (2019) also found that the environment appears to have a modest effect on the α -element abundances of galaxies, especially at low and average galaxy masses. Finally, as with stellar ages, although the global metallicity of galaxies correlates with their environment, metallicity gradients show weak or no environmental dependence (e.g. Goddard et al. 2017; Zheng et al. 2017).

In trying to understand the physical drivers of these differences, it is apparent that varying processes are at work depending on whether a galaxy is central within a halo or a satellite system. Indeed, analysing SDSS data, Peng et al. (2012) concluded that the quenching of satellite galaxies in galaxy groups provides the starting point of environmental effects. Kovač et al. (2014) further confirmed the dominant role of satellite quenching over time by analysing samples from zCOSMOS-bright data; they found little evidence that the red fraction of central galaxies depends on overdensity, while satellites are commonly redder at all overdensities, at least back to $z \sim 0.7$.

Currently, it is still unclear what distinction in physical mechanism is responsible for these differences in what is termed ‘environmental quenching’. A range of processes have been suggested that can contribute, which all involve depriving a galaxy of the cold gas that it needs to keep forming stars. For example, a galaxy may experience ram-pressure stripping when it moves through a hot gaseous medium, which can rapidly remove the fuel for star formation and quench the galaxy (e.g. Gunn & Gott 1972; Abadi, Moore & Bower 1999). Alternatively, if only the gas in the outer part of the galaxy is removed, or is prevented from falling to the galaxy through heating, the galaxy would experience ‘strangulation’ and gradually quench when the existing fuel is exhausted (e.g. Larson, Tinsley & Caldwell 1980; Balogh, Navarro & Morris 2000). Tidal interactions between galaxies in a group or between galaxies and the dark matter halo of the group or cluster can also cause stripping of the gas (e.g. Read et al. 2006). In each case, the net effect is the same, so the observable consequences of quenching will be similar, making it difficult to determine which processes are important in any particular situation. However, given the physical differences in these processes, we might expect to be able to distinguish between them on the basis of subtler indicators such as the time-scale over which star formation shuts down, and the way that gas loss can alter a galaxy’s chemical evolution.

Fortunately, we are now in a position to investigate these subtler factors to distinguish between such effects. The recently completed Mapping Nearby Galaxies at Apache Point Observatory (MaNGA) survey (Bundy et al. 2015) has provided us with high-quality spectra from a well-defined sample of over 10 000 nearby galaxies, which allows us to select a large set of galaxies in different environments, to search for quite subtle variations. The size of the survey also means that we can focus on a homogeneous subset of galaxies, matched in mass between environments, and chosen to have a shared underlying morphology – in this case, all disc galaxies – to seek to minimize the variations that might be expected for galaxies of very different types in different environments. Moreover, we have recently shown that, by fitting relatively simple stellar and chemical evolution models directly to the high-quality spectra that MaNGA provides, it is possible to determine physical parameters related to the time-scales of star formation and rates of gas accretion and loss that should allow us to distinguish between quenching mechanisms (Zhou, Merrifield & Aragón-Salamanca 2022, hereafter Paper I).

To this end, we have set out the analysis in this paper as follows. The data and sample selection, and a preliminary look at the evidence it presents for environmental influence, are described in Section 2. The ‘semi-analytic spectral fitting’ process, by which we fit a simple physically motivated evolutionary model directly to the spectra, is summarized in Section 3. The inferred evolutionary parameters for central, satellite, and isolated galaxies, and their implications for the drivers of environmental quenching, are described in Section 4. Finally, we summarize the key findings in Section 5.

2 DATA

2.1 The MaNGA survey

As part of the fourth generation of SDSS (SDSS-IV; Blanton et al. 2017), MaNGA has completed its mission to collect spatially resolved high-quality spectra for a well-defined sample of over 10 000 nearby galaxies (redshift $0.01 < z < 0.15$; Yan et al. 2016b; Wake et al. 2017). MaNGA targets were selected to span the stellar mass range $5 \times 10^8 \leq M_* \leq 3 \times 10^{11} h^{-2} M_\odot$ (Wake et al. 2017), using stellar masses from the NASA Sloan Atlas (NSA) catalogue¹ (Blanton et al. 2005a). Using two dual-channel BOSS spectrographs (Smee et al. 2013) mounted on the 2.5 m telescope (Gunn et al. 2006), intermediate-resolution ($R \sim 2000$; Drory et al. 2015) spectra that cover 3600–10 300 Å in wavelength were obtained out to at least 1.5 effective radii for all the target galaxies (Law et al. 2015). The raw spectra were reduced and calibrated (Yan et al. 2016a) via the Data Reduction Pipeline (Law et al. 2016) to produce science-ready spectra with flux calibrations better than 5 per cent across most of the wavelength range. The Data Analysis Pipeline (DAP; Belfiore et al. 2019; Westfall et al. 2019) processed these reduced data and provided the measurements of stellar kinematics, emission-line properties, and spectral indices employed in this work.

2.2 Sample selection and data reduction

The intent of this paper is to investigate how the stellar population properties in galaxies depend on the environment that they inhabit, specifically whether they are central or satellite galaxies in groups, or are isolated objects. To identify such systems, we make use of the 11th MaNGA Product Launch (MPL11) data, which comprise the full 10 010 unique galaxies observed, and were released with the SDSS-IV Data Release 17 (DR17; Abdurro’uf et al. 2022). We are also looking to select a sample in which mergers are unlikely to have confused the evolutionary picture significantly, so we focus on disc-like systems (Mo, Mao & White 1998). To this end, we make use of the value-added catalogue (VAC), the MaNGA Morphology Deep Learning DR17 Catalogue (Domínguez Sánchez et al. 2022), which provides classifications for all the MaNGA MPL11 galaxies. In this catalogue, several indicators are provided to describe the morphology of the galaxy. P_{LTG} is the probability of being late-type galaxies from the deep-learning approach. T-Type is another indicator with T-type ≤ 0 for early-type galaxies, T-type > 0 for late-type galaxies, and T-type = 0 for S0s. Visual class (VC) comes from visual inspection of the image of the galaxy, in which late-type galaxies are marked with VC = 3 and S0 with VC = 2. In addition, a visual classification flag (VF) is used to indicate the robustness of the visual classification, in which certain visual classification results have VF = 0. There are multiple ways in which these indicators can be combined to create a

¹ <http://www.nsatlas.org/>

single measure of morphology; here, we follow the criteria suggested in Domínguez Sánchez et al. (2022) to select disc galaxies as those in the VAC labelled with

- (i) spiral: ($P_{\text{LTG}} > 0.5$) and (T-Type > 0) and (VC = 3) and (VF = 0),
- (ii) S0: ($P_{\text{LTG}} < 0.5$) and (T-Type < 0) and (PS0 > 0.5) and (VC = 2) and (VF = 0),

which yields 5125 spirals and 891 S0s. To ensure the robustness of morphological classifications and to minimize dust attenuation effects, we also require the sample galaxies to be reasonably face-on; after applying an axial ratio cut of $b/a > 0.5$, we obtain a sample of 4416 reasonably face-on disc galaxies.

To obtain the requisite environment information, we make use of another VAC, the Galaxy Environment for MaNGA Value Added Catalog (GEMA-VAC). In this VAC, the environment information of MaNGA galaxies is derived using the methods described in Argudo-Fernández et al. (2015), Etherington & Thomas (2015), and Wang et al. (2016). The final catalogue will be described in more detail in Argudo-Fernández et al. (in preparation), but the VAC itself has been released with SDSS DR17. We use the group environment of MaNGA galaxies provided in the VAC, in which galaxies are allocated to groups using the catalogue of Yang et al. (2007). Using this information, we divide the sample into three classes:

- (i) isolated: number of galaxies $NG = 1$ in the group;
- (ii) central: the most massive galaxy in a group with $NG > 1$; and
- (iii) satellite: not the most massive galaxy in a group with $NG > 1$.

One further issue is that galaxies selected in different environments could have systematically different properties. In particular, their mass distributions are likely different, with more massive systems found in higher density regions. Since mass is likely the biggest single intrinsic driver of evolutionary differences, this effect would mask the extrinsic environmental effects that we are looking for. To mitigate this issue, we have mass-matched the subsamples of galaxies in each environmental category in the stellar mass range $9.5 < \log(M_*/M_\odot) < 11.5$. This range is divided into bins of width $\log(M_*/M_\odot) = 0.1$, which is approximately equal to the uncertainty in the mass measurement, and within each bin, we select all N galaxies from the least popular category, and a random subsample of N galaxies from the other two categories. In this way, we construct a mass-matched sample in the three categories, which ends up with 574 galaxies in each environmental class.

In this sample, most of the central galaxies come from relatively small groups, with a median number of group members $NG = 3$, and 90 per cent of the groups have $NG < 10$. Satellite galaxies come from bigger groups with a median $NG = 16$. In addition, the GEMA-VAC provides halo mass estimations for MaNGA galaxies obtained from Yang et al. (2007). We use these halo masses to characterize in more detail the dark matter halo properties of the sample galaxies. Isolated galaxies have halo masses in the range $10^{11.5} < M_h/M_\odot < 10^{13}$ with a median of $10^{12.4} M_\odot$. Central galaxies generally reside in relatively larger dark matter haloes with halo masses in the range $10^{11.5} < M_h/M_\odot < 10^{14}$ and a median of $10^{12.6} M_\odot$. As might be expected for satellite galaxies that do not define the mass of the halo in which they reside, the range for these systems is much larger, spanning from 10^{12} to $10^{14.5} M_\odot$ with a median of $10^{13.7} M_\odot$. In what follows, we will explore how this range of environments has affected the evolution of the galaxies they host.

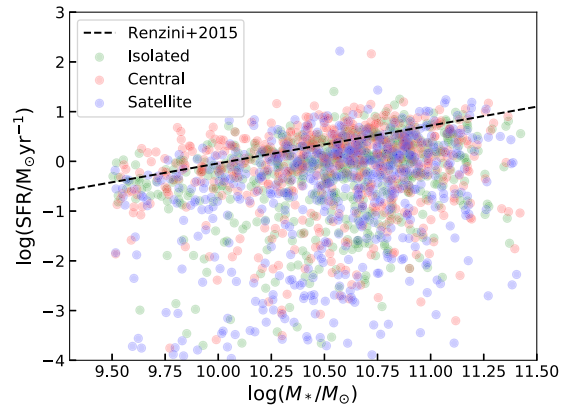


Figure 1. The SFR as a function of stellar mass for our sample galaxies. Isolated, central, and satellite galaxies are shown in green, red, and blue, respectively. The black dashed line shows the star-forming main sequence obtained by Renzini & Peng (2015) as reference.

2.3 Environmental dependence of the galaxies' empirical properties

Before getting into the detailed modelling that will tell us about the physical processes involved in environmental quenching, it is helpful to look for clues in the simpler empirical data available directly from the MaNGA DAP. In Fig. 1, we present the star formation activity of the sample galaxies as a function of their masses. For this analysis, we use $H\alpha$ flux measurements provided by MaNGA DAP (where detected) to estimate the star formation rate (SFR). Using the Calzetti extinction law (Calzetti et al. 2000) and assuming an intrinsic $H\alpha/H\beta$ ratio of 2.87 (Osterbrock & Ferland 2006), we correct the $H\alpha$ flux for dust attenuation. A conversion factor from Murphy et al. (2011) calibrated with a Chabrier (Chabrier 2003) initial mass function (IMF),

$$\frac{\text{SFR}}{M_\odot \text{ yr}^{-1}} = 5.37 \times 10^{-42} \frac{L(H\alpha)}{\text{erg s}^{-1}}, \quad (1)$$

is then applied to calculate the SFR, which is shown as a function of the stellar mass from the NSA. From the plot, we see that most of the sample galaxies lie close to the star-forming main sequence. However, significant deviations from the main sequence towards lower SFRs are also seen in many galaxies, particularly the satellite systems. Clearly, this offers evidence that the present-day SFRs in disc galaxies are significantly affected by environment.

To probe further back into the SFHs of galaxies of different types, we can look for empirical evidence in various absorption-line indices that have been measured for these galaxies. In particular, the Dn4000 index is often used as an indicator of the stellar population, and specifically a value of $\text{Dn4000} < 1.6$ will be an indicator of star formation within the past 1–2 Gyr (e.g. Kauffmann et al. 2003). In addition, the $\text{Mgb}/(\text{Fe}) \equiv \text{Mgb}/(0.5 * \text{Fe5270} + 0.5 * \text{Fe5335})$ index is a proxy for the relative abundance of α elements, for which higher values are found in galaxies whose stars formed on a shorter time-scale (e.g. Worthey 1994; Thomas et al. 2005; Zheng et al. 2019). Fig. 2 shows the average values for these indices, integrated out to the effective radius of all the sample galaxies, as a function of their stellar masses. Although there is a good deal of scatter, the average lines on these plots show clear systematic differences between galaxies in different environments. The satellite galaxies show stronger values of both indices, indicating relatively little recent star formation, consistent with what we have learned from $H\alpha$, and a shorter time-scale for their formation. Interestingly, though, we

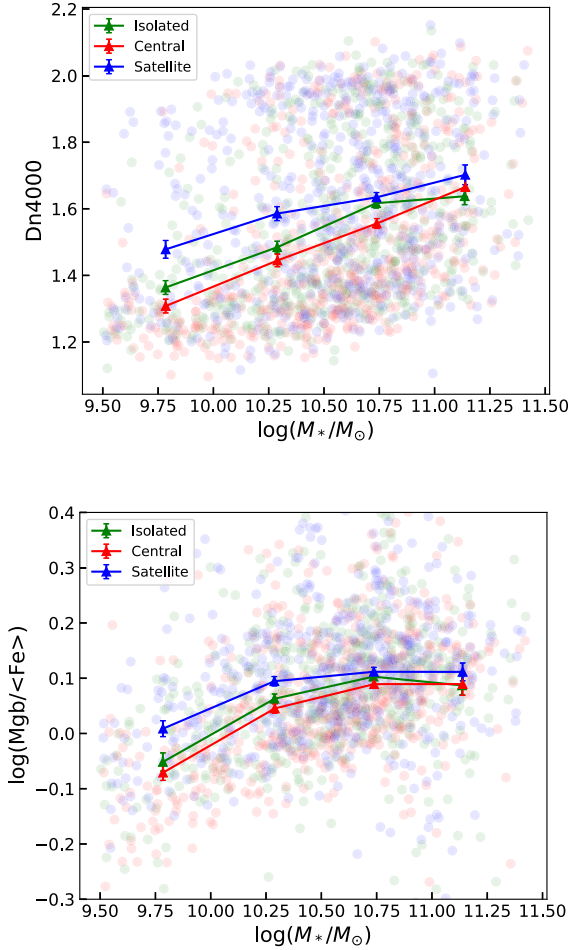


Figure 2. Dn4000 (top panel) and Mgb/⟨Fe⟩ (bottom panel) as functions of stellar mass for our sample galaxies. Isolated, central, and satellite galaxies are shown in green, red, and blue, respectively. Triangles linked by lines are mean results in different stellar mass bins, with error bar showing the error estimated from the jackknife resampling method.

also see consistent, if subtle, differences between central and isolated galaxies, even in these relatively crude measures of galaxy evolution, which motivates a more thorough investigation of its causes.

3 ANALYSIS

3.1 The chemical evolution model

In order to investigate the physical processes that underlie the spectral differences between galaxies in different environment, we fit a chemical evolution model directly to the spectra. The model is designed to be sufficiently general to capture the main physical processes in a wide variety of formation scenarios, but simple enough to produce robust fits to the spectra. This semi-analytic spectral fitting approach is described in detail in Paper I, but we summarize the main steps in the approach here.

To construct a sufficiently general picture of the star formation and chemical evolution of a galaxy, we have to take into account gas inflow and outflow processes as well as the star formation triggered by the resulting gas reservoir. We therefore consider a model in which the gas mass evolution of the galaxy can be described by

$$\dot{M}_g(t) = \dot{M}_{\text{in}}(t) - \psi(t) + \dot{M}_{\text{re}}(t) - \dot{M}_{\text{out}}(t). \quad (2)$$

The first term characterizes the gas inflow, which is assumed to have an exponentially decaying form

$$\dot{M}_{\text{in}}(t) = Ae^{-(t-t_0)/\tau}, \quad t > t_0. \quad (3)$$

The second term represents the gas lost to star formation, with the third term accounting for the mass ejection from dying stars, and the final term describing mass lost from the system. We assume a linear Schmidt law (Schmidt 1959) to model the star formation activity, so

$$\psi(t) = S \times M_g(t), \quad (4)$$

where S is the star formation efficiency. We assume this efficiency to be constant throughout the evolution and estimate it with the extended Schmidt law proposed by Shi et al. (2011),

$$S(\text{yr}^{-1}) = 10^{-10.28 \pm 0.08} \left(\frac{\Sigma_*}{M_\odot \text{pc}^{-2}} \right)^{0.48}, \quad (5)$$

where Σ_* is the stellar mass surface density of the galaxy. We obtain an approximate average value for Σ_* from the current stellar mass and effective radius in the NSA, $\Sigma_* = 0.5 \times M_*/(\pi R_e^2)$.

In this model, a constant mass return fraction of $R = 0.3$ is assumed, so that the stars formed in each generation will return 30 per cent of their stellar masses to the ISM. For the mass-loss term, we follow the canonical assumption that the outflow strength is proportional to the star formation activity:

$$\dot{M}_{\text{out}}(t) = \lambda \psi(t), \quad (6)$$

where the dimensionless quantity λ is the relative outflow strength, often called the ‘wind parameter’.

In Paper I, we assumed the outflow to be constant, but with a sharp cut-off at some time (to represent when a galaxy’s potential well became too deep for the winds to escape). This assumption allows a secondary star formation episode during the evolution of the galaxy, but the sudden cut-off leads to discontinuity in the chemical and star formation evolution. Here, we consider a somewhat gentler model for the changes in the wind parameter, which is assumed to vary linearly between an initial value λ_b at the beginning of galaxy formation (14 Gyr ago) and a value of λ_e at the present day:

$$\lambda(t) = \lambda_b + (\lambda_e - \lambda_b)t/(14 \text{ Gyr}). \quad (7)$$

We found that this simple refinement avoids the likely unphysical discontinuity in properties, while leaving the statistical results largely unchanged. Using all those ingredients, the equation that characterizes the gas mass evolution can be written as

$$\dot{M}_g(t) = Ae^{-(t-t_0)/\tau} - S(1 - R + \lambda(t))M_g(t). \quad (8)$$

For the chemical evolution, we adopt the usual instantaneous mixing approximation, in which the gas in a galaxy is always well mixed during its evolution. The equation that characterizes the chemical evolution can then be written as

$$\begin{aligned} \dot{M}_Z(t) = & Z_{\text{in}}Ae^{-(t-t_0)/\tau} - Z_g(t)(1 - R)SM_g(t) \\ & + y_Z(1 - R)SM_g(t) - Z_g(t)\lambda(t)SM_g(t), \end{aligned} \quad (9)$$

where $Z_g(t)$ is the gas-phase metallicity and $M_Z(t) \equiv M_g \times Z_g$. The first term is the inflow, which brings in gas with metallicity Z_{in} , which is simply assumed to be $Z_{\text{in}} = 0$ throughout this work. The second term characterizes the metal locked up in long-lived stars, while the third term represents the metal-enriched gas returned by dying stars. The last term characterizes how the outflow blows away metal-enriched gas, with a time-dependent outflow strength specified by equation (7).

Table 1. Priors of model parameters used to fit galaxy spectra.

Parameter	Description	Prior range
y_Z	Yield parameter	[0.0, 0.08]
τ	Gas infall time-scale	[0.0, 14.0] Gyr
t_0	Start time of gas infall	[0.0, 14.0] Gyr
λ_b	The wind parameter 14 Gyr ago	[0.0, 10.0]
λ_e	The current wind parameter	[0.0, 10.0]
$E(B - V)$	Dust attenuation parameter	[0.0, 0.5]

3.2 Fitting the model to observed data

Now that we have a very general model for the SFH and chemical evolution history (ChEH) of a galaxy, we are in a position to constrain its parameters using the spectral data from each galaxy. We do so by adopting a Bayesian framework, using an updated version of the Bayesian Inference of Galaxy Spectra (BIGS), as presented in Paper I. In short, a set of model parameters are generated from an appropriate prior distribution (listed in Table 1), which are used to calculate the SFH and ChEH following equations (8) and (9). The present-day gas-phase metallicity Z_g is obtained from the ChEH. Using the Bruzual & Charlot (2003) stellar population models, we calculate a model spectrum corresponding to the SFH and ChEH following the standard stellar population synthesis approach (see review by Conroy 2013). We use Bruzual & Charlot (2003) models constructed with the ‘Padova1994’ isochrones, the Chabrier (Chabrier 2003) IMF, and the STILIB (Le Borgne et al. 2003) stellar templates, which covers metallicities from $Z = 0.0001$ to $Z = 0.05$, and ages from 0.0001 Gyr to 20 Gyr. The library models have a full width at half-maximum resolution of 3 \AA in the wavelength range 3200–9500 \AA , which makes them well suited to fitting MaNGA spectra observed at 3600–10 300 \AA with low redshifts ($z \sim 0.03$; Wake et al. 2017), but we must also broaden the stellar templates to match the broadening due to stellar velocity dispersion and instrumental effects, which we infer from an initial PXP fit to the spectra (Cappellari 2017). We can then compare the inferred model spectrum to the MaNGA data and vary the parameters to find the best-fitting physically motivated model.

This method was extensively tested in Paper I, in which we showed that, with spectral data at a sufficient signal-to-noise ratio (S/N), it can reliably reproduce the overall SFH and ChEH of galaxies even when the simplified model does not exactly match the detailed history of a galaxy. However, it does require quite a high S/N to fit reliably. Fortunately, here we are interested in the global properties of galaxies, so, as described in Paper I, can combine all the data within $1R_e$ of each galaxy to obtain a spectrum with an S/N of ~ 70 per \AA , which is sufficient to robustly reproduce the system’s history.

In Paper I, we used emission-line diagnostics to further constrain the present-day SFR and gas-phase metallicity. In this work, however, as we no longer focus only on spiral galaxies, some objects do not offer these constraints. However, we can use a population-wide relation instead, at least for the metallicity constraint. Specifically, Andrews & Martini (2013) demonstrated that there is quite a tight relationship between mass and gas-phase metallicity, so we can assign an expected gas-phase oxygen abundance using

$$12 + \log(\text{O}/\text{H}) = 8.798 - \log \left(1 + \left(\frac{10^{8.901}}{M_*/M_\odot} \right)^{0.64} \right). \quad (10)$$

This oxygen abundance is then converted into total metallicity using a solar metallicity of 0.02 and oxygen abundance of $12 + \log(\text{O}/\text{H}) =$

8.83 (Anders & Grevesse 1989). We note that this relation is chosen to be consistent with the calibration of the Bruzual & Charlot (2003) single stellar population (SSP) models; alternative calibrations can also be applied, but appropriate caution is urged when comparing with our results. The likelihood function used in deriving a best fit can then be written as

$$\ln L(\theta) \propto - \sum_i^N \frac{(f_{\theta,i} - f_{D,i})^2}{2f_{\text{err},i}^2} - \frac{(Z_{g,\theta} - Z_{g,D})^2}{2\sigma_Z^2}, \quad (11)$$

where $f_{\theta,i}$ is the flux predicted from the model with parameter set θ , while $f_{D,i}$ is the observed flux from the stacked spectrum. $f_{\text{err},i}$ represents the corresponding error spectrum, and the sum is made over all N wavelength points. $Z_{g,\theta}$ is the current gas-phase metallicity from the model, while $Z_{g,D}$ is the gas-phase metallicity estimated from the empirical relation of equation (10). σ_Z is the uncertainty in the gas-phase metallicity estimates, which was set to $\sigma_Z = 0.1Z_{g,D}$ (Paper I).

4 RESULTS AND DISCUSSION

Having performed the semi-analytic spectral fitting on the full mass-matched sample of central, satellite, and isolated galaxies, we are now in a position to quantify and interpret, at least in broad terms, the empirical differences in their properties found in Section 2.3 in terms of the basic physical parameters that this analysis provides. In Fig. 3, we present the average derived properties and underlying physical parameters for the mass-matched samples of isolated, central, and satellite galaxies, divided into four mass bins. We present these properties in cumulative form, in part because in some cases it has a simpler physical interpretation (e.g. Greener et al. 2021), but also because it makes clearer the systematic differences between the subsamples.

In terms of SFH (top row of Fig. 3), it is clear that in the lowest stellar mass bin ($10^{9.5} < M_*/M_\odot < 10^{10.0}$), central galaxies accumulate their stellar mass significantly later than satellite galaxies: On average less than 30 per cent of the stellar mass in central galaxies formed earlier than 5 Gyr ago, while in the same period, satellite galaxies had accumulated more than 60 per cent of their stellar mass. The evolutionary history of isolated galaxies lies between these two extremes. These SFHs are in line with indications from the lower panel of Fig. 2, in which the higher α -element abundance in low-mass satellites flags their shorter star formation time-scales. The difference between central and satellite galaxies becomes weaker in higher mass galaxies, and in galaxies with $M_*/M_\odot > 10^{10.5}$, the difference is almost negligible. The different formation history of central and satellite galaxies, as well as its variation with stellar mass, is consistent with previous investigations (e.g. Pasquali et al. 2010; Peng et al. 2012; Wetzel et al. 2012), but the evolutionary model fitted here means that we will be able to go on to attribute a physical interpretation to these differences.

The second row of Fig. 3 shows the associated average cumulative metallicity distribution function (CMDF) in the different mass bins. Once again, it is the low-mass galaxies that display the biggest differences, with satellite galaxies having ~ 80 per cent of stars with $Z < 0.005$, while in central galaxies of similar stellar mass, this fraction decreases to ~ 20 per cent. The low-metal-rich CMDF of low-mass satellite galaxies is characteristic of the so-called closed-box or leaky-box model, in which there is no significant gas infall to the system (Tinsley 1974); in contrast, the CMDFs in central galaxies are closer to the predictions of ‘accreting box’ models (Tinsley 1974, 1980), in which a replenishing supply of new gas is provided, which

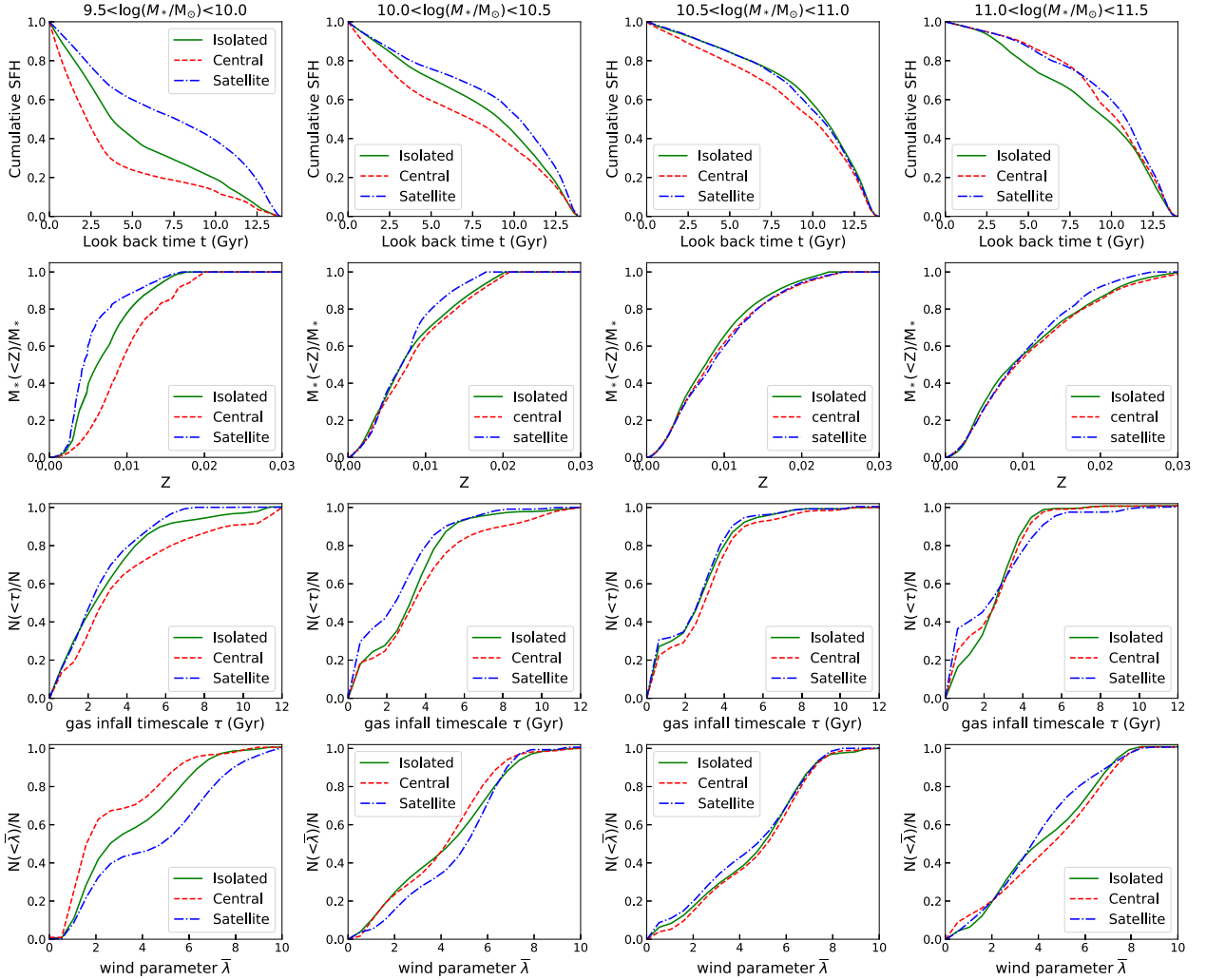


Figure 3. Environment dependence of galaxy properties derived from best-fitting models for our sample galaxies. The first row shows the cumulative SFH, while the second row shows the cumulative metallicity distribution, averaged over galaxies in each bin and category, respectively. To interpret the derived mass and chemical evolution, the third and fourth panels show the cumulative distributions of the gas infall time-scale τ and mass-weighted averaged wind parameter $\bar{\lambda}$, as indicators of gas infall and outflow properties, respectively, in our sample galaxies. In each row, from left to right, different panels show results from different stellar mass bins as indicated. In each panel, green, red, and blue lines show the results obtained from isolated, central, and satellite galaxies, respectively.

suppresses the relative fraction of low-metallicity stars. This effect is still present in higher mass bins, but is much reduced, indicating that environment is a much less important factor in the chemical evolution of these galaxies.

We can now quantify plausible drivers of these differences using the physical parameters inferred in the semi-analytic spectral fitting process. The third row of Fig. 3 shows one of the primary drivers of differences between galaxies, the gas infall time-scale, as a function of both environment and mass. It is apparent that, at low and intermediate masses, central galaxies tend to have longer gas infall time-scales, while the gas infall occurs over a systematically shorter period in satellite galaxies. In the lowest-mass bin ($10^{9.5} < M_*/M_\odot < 10^{10.0}$), almost all of the satellite galaxies have gas infall time-scales less than ~ 5 Gyr, while around 40 per cent of central galaxies have time-scales greater than ~ 5 Gyr, with isolated galaxies somewhere in between. The median gas infall time-scales for satellite, isolated, and central galaxies are 2.6, 2.9, and 3.9 Gyr, respectively. In more massive galaxies ($M_*/M_\odot > 10^{10.5}$), these

differences become less systematic: The median gas infall time-scales for all the three categories becomes shorter, and all converge to around 2.5 Gyr in the highest-mass bin ($10^{11} < M_*/M_\odot$). Such variations with stellar mass are in line with the down-sizing formation scenario, with time-scales compressed for more massive objects. In addition, the environment effects found in low-mass galaxies fit with suggested physical mechanisms for quenching galaxy formation, in which satellites falling into a larger dark matter halo can experience the removal of their hot gaseous halo through tidal ‘strangulation’ processes (Balogh et al. 2000; Pasquali et al. 2010) or even the direct ram-pressure stripping of their cold star-forming gas (Gunn & Gott 1972; Abadi et al. 1999), resulting in an early end to their gas supply. The fitted time-scales for gas depletion in satellites in Fig. 3 are relatively long (~ 3 Gyr), which argues for the gentler process of strangulation, consistent with the conclusions from entirely independent lines of evidence reached by van den Bosch et al. (2008), Pasquali et al. (2010), and Peng, Maiolino & Cochrane (2015).

One other interesting phenomenon apparent in the distribution of τ in Fig. 3 is the step in its cumulative distribution that is particularly apparent in more massive galaxies. This feature represents a separate population of galaxies in which the gas infall time-scale is less than ~ 1 Gyr. Further investigation of these galaxies reveals that they are almost all classified as S0 or lenticular galaxies. These systems accumulated their stellar masses very early, so are barely resolved in the current analysis. It is none the less interesting to note that they make up a higher fraction of satellite than central galaxies, again implying that the process responsible for their creation is dependent on environment.

The other major component in the semi-analytic model is outflow, as described by the wind parameter λ . Since this parameter is allowed to vary over the lifetime of each galaxy, we quantify it in each system using an average value that reflects when it will have most affected the SFH of the galaxy,

$$\bar{\lambda} \equiv \frac{\int_0^{t_u} \psi(t)\lambda(t)dt}{\int_0^{t_u} \psi(t)dt}, \quad (12)$$

where $\psi(t)$ is the SFR at time t and $t_u = 14.0$ Gyr is the age of the Universe. The bottom row of Fig. 3 shows how this average wind parameter varies with galaxy mass and environment. Once again, it is only in the lowest-mass galaxies where we see a significant effect, with satellite galaxies showing much stronger wind parameters than central ones, with isolated galaxies somewhere in between. The median average wind parameters for satellite, isolated, and central galaxies in the lowest-mass bin ($10^{9.5} < M_*/M_\odot < 10^{10.0}$) are 4.5, 3.5, and 2.6, respectively, while in relatively massive galaxies ($10^{10} < M_*/M_\odot$), the median values all converge to around 4. Although this parameter was formulated in terms of a star formation-driven wind, it really just measures the effectiveness of the loss of processed gas from the galaxy. The relatively high rate of loss from satellites therefore fits with a picture in which a system falling into a more massive halo might be expected to lose its own extended halo of hot processed gas through interaction with other group members (Gunn & Gott 1972; Abadi et al. 1999). Similarly, the greater ability of a central galaxy to hold on to this processed gas when compared to an isolated system presumably reflects the deeper potential well in which it sits. The disappearance of difference between the wind parameters in galaxies with stellar masses higher than $10^{10.0} M_\odot$ implies that massive satellite galaxies do not lose more gas than centrals. This convergence in properties can likely be attributed to the greater ability of massive galaxies to hold on to processed gas against external influences, so that their evolution is mostly determined by internal processes rather than their environment.

In summary, after controlling for mass, we find strong evidence for environmental influence in the ChEH and SFH of disc galaxies, particularly in low-mass systems. We can also quantify these differences in terms of the underlying physical processes of pristine gas accretion and processed gas loss, in the sense that low-mass satellites have their gas accretion shut off at an earlier stage, and are more likely to lose their processed gas rather than recycling it into further generations of stars. We also find a clear difference between central and isolated galaxies, in that central galaxies continue to accrete gas over longer time-scales, and are better at holding on to that gas once processed through a generation of stars. We note that these physically plausible differences were not at all imposed by the semi-analytic spectral fitting process, which had no way of knowing whether a particular spectrum came from a central, satellite, or isolated galaxy. The differences therefore seem to be astrophysical in origin, and offer

further confirmation of the reliability of this archaeological approach to studying galaxy evolution.

5 CONCLUSIONS

In this work, we have applied the semi-analytic spectral fitting approach to a sample of disc galaxies selected from the SDSS-IV/MaNGA survey to investigate the dependence of such galaxies' evolution on their environment. The sample is comprised of three mass-matched sets of isolated, central, and satellite galaxies, the latter two categories defined by whether or not the galaxy is the most massive member of a group. The data for each galaxy within one effective radius were combined to create a high-S/N spectrum representing the system's global properties. The semi-analytic spectral fitting process not only reproduces the properties of the spectrum by fitting an SFH and a ChEH, but also determines physical parameters of gas accretion and outflow that generate the model. From these fits, we have determined that:

(i) The cumulative SFHs derived from the sample galaxies reveal an earlier cessation of star formation activities in low-mass ($10^{9.5} < M_*/M_\odot < 10^{10.0}$) satellite galaxies than their central equivalents: Less than 40 per cent of the stellar masses in satellite galaxies formed within the most recent 5 Gyr, while central galaxies of similar mass accumulated more than 70 per cent of their stellar masses over the same period. Isolated galaxies have intermediate properties. This environmental dependence becomes weaker in more massive galaxies, and essentially disappears for systems with $M_*/M_\odot > 10^{10.5}$. These differences also fit with a more qualitative analysis looking at the abundances of α elements in different galaxies, with low-mass satellites showing the sort of α enhancement associated with a briefer period of star formation.

(ii) The environmental dependence of disc galaxy evolution, as well as its mass dependence, is also seen in the chemical evolution of the galaxies. Low-mass ($10^{9.5} < M_*/M_\odot < 10^{10.0}$) satellite galaxies contain a high fraction of low-metallicity stars compared to central galaxies, indicating that they are more likely to be 'closed-box' or 'leaky-box' systems, while central galaxies of similar masses contain lower fractions of low-metallicity stars, suggesting that ongoing accretion played a more important role in their formation. Once again, isolated galaxies lie between central and satellite galaxies, and environmental dependence becomes negligible in galaxies more massive than $\sim 10^{10.5} M_\odot$.

(iii) The gas accretion history inferred from the semi-analytic fitting process drives the variations in time-scale: In low-mass central galaxies, the average gas infall time-scale is found to be systematically longer than comparable satellite galaxies, leading to their more extended SFHs. Again, this variation disappears in more massive galaxies, where we also start to see a different subpopulation of S0 galaxies, whose gas was accreted over a very short time-scale. However, the time-scales are not that short for the low-mass satellite systems, suggesting the slow 'strangulation' of their star formation caused by the removal of their extended hot halo of gas rather than more abrupt ram-pressure stripping.

(iv) This scenario is further supported by the inferred mass-loss parameters in low-mass galaxies, where satellite systems are found to have stronger wind parameters, indicating that their processed gas has been effectively removed. By contrast, central galaxies have weaker wind parameters than their isolated equivalents, as would be expected if the deeper potential well of a group were better at retaining such processed material.

The consistent story obtained from the semi-analytic spectral fitting process offers real confidence that even the simple chemical evolution model adopted, with its parametrization of gas accretion and mass-loss, provides a credible physical description of the histories of these galaxies. This new direct model fitting approach, combined with the large sample size and high-quality data in the MaNGA survey, has revealed the significant impact of environment on lower mass galaxies, and allowed us to quantify it in a way that has not been possible previously.

ACKNOWLEDGEMENTS

SZ, MRM, and AAS acknowledge financial support from the UK Science and Technology Facilities Council (STFC; grant ref: ST/T000171/1).

For the purpose of open access, the authors have applied a creative commons attribution (CC BY) to any journal-accepted manuscript.

Funding for the Sloan Digital Sky Survey IV has been provided by the Alfred P. Sloan Foundation, the U.S. Department of Energy Office of Science, and the Participating Institutions. SDSS-IV acknowledges support and resources from the Center for High-Performance Computing at the University of Utah. The SDSS website is www.sdss.org.

SDSS-IV is managed by the Astrophysical Research Consortium for the Participating Institutions of the SDSS Collaboration, including the Brazilian Participation Group, the Carnegie Institution for Science, Carnegie Mellon University, the Chilean Participation Group, the French Participation Group, Harvard-Smithsonian Center for Astrophysics, Instituto de Astrofísica de Canarias, The Johns Hopkins University, Kavli Institute for the Physics and Mathematics of the Universe (IPMU)/University of Tokyo, Lawrence Berkeley National Laboratory, Leibniz Institut für Astrophysik Potsdam (AIP), Max-Planck-Institut für Astronomie (MPIA Heidelberg), Max-Planck-Institut für Astrophysik (MPA Garching), Max-Planck-Institut für Extraterrestrische Physik (MPE), National Astronomical Observatories of China, New Mexico State University, New York University, University of Notre Dame, Observatório Nacional/MCTI, The Ohio State University, Pennsylvania State University, Shanghai Astronomical Observatory, United Kingdom Participation Group, Universidad Nacional Autónoma de México, University of Arizona, University of Colorado Boulder, University of Oxford, University of Portsmouth, University of Utah, University of Virginia, University of Washington, University of Wisconsin, Vanderbilt University, and Yale University.

DATA AVAILABILITY

The data underlying this paper were accessed from SDSS DR17 (<https://www.sdss.org/dr17/manga/>). The derived data generated in this research will be shared on request to the corresponding author.

REFERENCES

- Abadi M. G., Moore B., Bower R. G., 1999, *MNRAS*, 308, 947
 Abdurro'uf et al., 2022, *ApJS*, 259, 35
 Anders E., Grevesse N., 1989, *Geochim. Cosmochim. Acta*, 53, 197
 Andrews B. H., Martini P., 2013, *ApJ*, 765, 140
 Argudo-Fernández M. et al., 2015, *A&A*, 578, A110
 Baldry I. K., Balogh M. L., Bower R. G., Glazebrook K., Nichol R. C., Bamford S. P., Budavari T., 2006, *MNRAS*, 373, 469
 Balogh M. L., Navarro J. F., Morris S. L., 2000, *ApJ*, 540, 113
 Belfiore F. et al., 2019, *AJ*, 158, 160
 Blanton M. R. et al., 2005a, *AJ*, 129, 2562
 Blanton M. R., Eisenstein D., Hogg D. W., Schlegel D. J., Brinkmann J., 2005b, *ApJ*, 629, 143
 Blanton M. R. et al., 2017, *AJ*, 154, 28
 Bruzual G., Charlot S., 2003, *MNRAS*, 344, 1000
 Bundy K. et al., 2015, *ApJ*, 798, 7
 Calzetti D., Armus L., Bohlin R. C., Kinney A. L., Koornneef J., Storchi-Bergmann T., 2000, *ApJ*, 533, 682
 Cappellari M., 2017, *MNRAS*, 466, 798
 Chabrier G., 2003, *PASP*, 115, 763
 Conroy C., 2013, *ARA&A*, 51, 393
 Darvish B., Mobasher B., Sobral D., Rettura A., Scoville N., Faisst A., Capak P., 2016, *ApJ*, 825, 113
 Domínguez Sánchez H., Margalef B., Bernardi M., Huertas-Company M., 2022, *MNRAS*, 509, 4024
 Dressler A., 1980, *ApJ*, 236, 351
 Drory N. et al., 2015, *AJ*, 149, 77
 Etherington J., Thomas D., 2015, *MNRAS*, 451, 660
 Goddard D. et al., 2017, *MNRAS*, 465, 688
 Greener M. J., Merrifield M., Aragón-Salamanca A., Peterken T., Andrews B., Lane R. R., 2021, *MNRAS*, 502, L95
 Gunn J. E., Gott J., Richard I., 1972, *ApJ*, 176, 1
 Gunn J. E. et al., 2006, *AJ*, 131, 2332
 Kauffmann G. et al., 2003, *MNRAS*, 341, 33
 Kauffmann G., White S. D. M., Heckman T. M., Ménard B., Brinchmann J., Charlot S., Tremonti C., Brinkmann J., 2004, *MNRAS*, 353, 713
 Kawinwanichakij L. et al., 2017, *ApJ*, 847, 134
 Kovač K. et al., 2014, *MNRAS*, 438, 717
 Larson R. B., Tinsley B. M., Caldwell C. N., 1980, *ApJ*, 237, 692
 Law D. R. et al., 2015, *AJ*, 150, 19
 Law D. R. et al., 2016, *AJ*, 152, 83
 Le Borgne J.-F. et al., 2003, *A&A*, 402, 433
 Li C., Kauffmann G., Jing Y. P., White S. D. M., Börner G., Cheng F. Z., 2006, *MNRAS*, 368, 21
 Mo H. J., Mao S., White S. D. M., 1998, *MNRAS*, 295, 319
 Murphy E. J. et al., 2011, *ApJ*, 737, 67
 Oemler A., Jr, 1974, *ApJ*, 194, 1
 Osterbrock D. E., Ferland G. J., 2006, *Astrophysics of Gaseous Nebulae and Active Galactic Nuclei*. University Science Books, Sausalito, CA
 Pasquali A., Gallazzi A., Fontanot F., van den Bosch F. C., De Lucia G., Mo H. J., Yang X., 2010, *MNRAS*, 407, 937
 Peng Y.-j. et al., 2010, *ApJ*, 721, 193
 Peng Y.-j., Lilly S. J., Renzini A., Carollo M., 2012, *ApJ*, 757, 4
 Peng Y., Maiolino R., Cochrane R., 2015, *Nature*, 521, 192
 Postman M., Geller M. J., 1984, *ApJ*, 281, 95
 Read J. I., Wilkinson M. I., Evans N. W., Gilmore G., Kleyna J. T., 2006, *MNRAS*, 366, 429
 Renzini A., Peng Y.-j., 2015, *ApJ*, 801, L29
 Sánchez-Blázquez P., Gorgas J., Cardiel N., González J. J., 2006, *A&A*, 457, 809
 Schmidt M., 1959, *ApJ*, 129, 243
 Shi Y., Helou G., Yan L., Armus L., Wu Y., Papovich C., Stierwalt S., 2011, *ApJ*, 733, 87
 Smeed S. A. et al., 2013, *AJ*, 146, 32
 Spindler A. et al., 2018, *MNRAS*, 476, 580
 Thomas D., Maraston C., Bender R., Mendes de Oliveira C., 2005, *ApJ*, 621, 673
 Tinsley B. M., 1974, *ApJ*, 192, 629
 Tinsley B. M., 1980, *Fundam. Cosm. Phys.*, 5, 287
 van den Bosch F. C., Aquino D., Yang X., Mo H. J., Pasquali A., McIntosh D. H., Weinmann S. M., Kang X., 2008, *MNRAS*, 387, 79
 Wake D. A. et al., 2017, *AJ*, 154, 86
 Wang H. et al., 2016, *ApJ*, 831, 164
 Westfall K. B. et al., 2019, *AJ*, 158, 231
 Wetzel A. R., Tinker J. L., Conroy C., 2012, *MNRAS*, 424, 232
 Wetzel A. R., Tinker J. L., Conroy C., van den Bosch F. C., 2013, *MNRAS*, 432, 336
 White S. D. M., Rees M. J., 1978, *MNRAS*, 183, 341

Worthey G., 1994, *ApJS*, 95, 107

Yan R. et al., 2016a, *AJ*, 151, 8

Yan R. et al., 2016b, *AJ*, 152, 197

Yang X., Mo H. J., van den Bosch F. C., Pasquali A., Li C., Barden M., 2007, *ApJ*, 671, 153

York D. G. et al., 2000, *AJ*, 120, 1579

Zheng Z. et al., 2017, *MNRAS*, 465, 4572

Zheng Z. et al., 2019, *ApJ*, 873, 63

Zhou S., Merrifield M., Aragón-Salamanca A., 2022, *MNRAS*, 513, 5446 (Paper I)

This paper has been typeset from a $\text{\TeX}/\text{\LaTeX}$ file prepared by the author.